Study on the Mechanism of Particle Breakage under New Composite Loads

Zhanfu Li[1,2], Yiqing Ye[1], Xin Tong[1,]*& Kunyuan Li[1]

[1]Mechanical Engineering training base, School of Mechanical and Automobile Engineering, Fujian University of Technology, Fuzhou, China
[2]China State Construction Engineering Corporation, Fuzhou, China
*E-mail: Tongxin_hqu_fjut@163.com

Abstract. A theoretical model of particle breakage under a novel combination of dynamic and static loads is presented in this paper. In order to enhance the capability of the actual physical and mechanical properties towards rocks, parallel connector parameters of a bonded particle model (BPM) from the discrete element method (DEM) were investigated by uniaxial compression tests. Then, the efficiency evaluation index system of particle breakage was defined and different simulations of various parameters were set, i.e. the speed of the moving plate, the curvature of the moving plate, the curvature of the fixed plate, the space between the two plates, and the initial particle radius. The mechanism of particle breakage was analyzed by the relationships between the efficiency evaluation index and various parameters. The investigation of particle breakage theory and law can help to design and improve crushing equipment, reduce the energy consumption of the crusher, and improve the quality of the broken product.

Keywords: *bonded particle model; breakage behavior; discrete element method; energy consumption; particle breakage.*

1 Introduction

As basic material for concrete, mortar and cement products, manufactured sand plays an increasingly significant role in the construction industry, the railway industry and the water conservancy industry. The crusher is the most efficient instrument to produce manufactured sand. Two loading modes are commonly used separately: static load and dynamic load. The jaw crusher, the cone crusher and the roller crusher mostly use static compression load. Dynamic impactive crushing equipment includes the hammer crusher, the impact crusher, the vertical shaft impact crusher, and so on. Different equipment and loading modes are shown in Figure 1 [1-3]. In order to improve crushing behavior, this paper proposes a new load mode that couples static and dynamic load patterns. This paper enriches the theory of breakage analysis and its mechanism was studied to lay the foundations for a new type of crushing machine.

Received September 14th, 2018, Revised January 5th, 2018, Accepted for publication March 13th, 2019.
 ISSN: 2337-5779, DOI: 10.5614/j.eng.technol.sci.2019.51.2.6

In recent years, experimental and simulation investigations into breakage index, breakage efficiency, breakeage energy and particle size distribution using instruments (uniaxial compression [4,5], drop hammer impact machine [6-8], and dynamic Hopinson bar impact [9-10]) and numerical simulation have been conducted by several researchers [11-13]. Kamali-Asl, *et al.* have investigated the effects of anisotropy on the mechanical response of one vertically-drilled and one horizontally-drilled sub-core that were extracted from a phyllite core [14]. Kamali-Asl, *et al.* characterized shale gas rock to improve the constitutive and numerical modeling [15]. DEM is increasingly used to study the crushing process of rocks modeled by BPMs. The results correspond well with the behaviors of real rock [16,17].

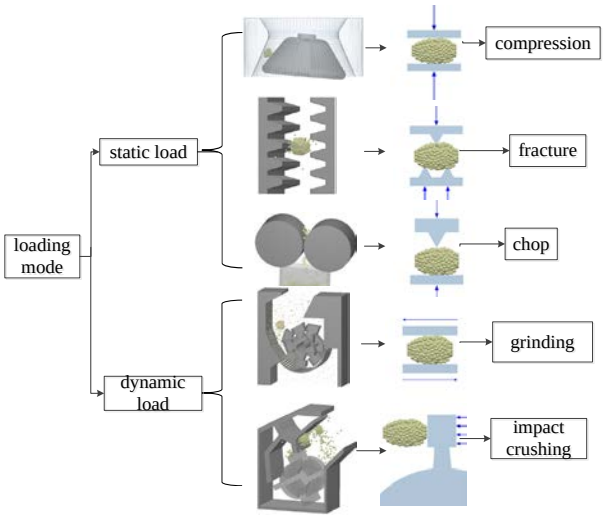

Figure 1 Breaking mode and crushing equipment.

A BPM is composed of a pile of small particles with parallel connection bonds that reflect force and moment. When the BPM reaches the stress limit of an external force, the parallel connection bonds break. Hence, the parameters of the bonds have a significant influence on the accuracy of the crushing result [18,19]. Several researchers have studied these parameters to match the real crushing process. Zhao [20] and others summarized calculation formula on microscopic parameters of parallel connection bonds without concluding the particle accumulation form. Zhang [21] ran calibrated particle connection parameters using a virtual test and then rebuilt the particle connection model. When the arrangement of the particles was changed, the parameters did not match. Legendre and Quis [22-23] calibrated the parameters when the particle connection model intersected with the accumulated granules and the workload

was large. The existing particle connection method and the connection parameters need to be deeply improved to achieve a reasonable bonded particle model that can reflect the physical properties of real rock. In this paper, the proposed bonded-particle model and the parameters of the parallel connection bonds were verified using a uniaxial compression simulation test. This paper also proposes a composite loading model and defines a particle crushing efficiency evaluation index system. The relationship between the different crushing parameters and the efficiency evaluation index were analyzed using DEM-simulations to describe the mechanism of particle breakage and enrich the theory of breakage analysis.

2 Construct Bonded-particle Model

Unit area normal stiffness, unit area shear stiffness, critical normal stress, critical tangential stress and connection bond radius affect the reliability of the simulation. In order to obtain reasonable compressive strength and elasticity modulus values, this paper set up a uniaxial compression 3D-model of the test specimen and then this model was verified using an electronic universal testing machine. Finally, a new 3D-model for crushing simulation was derived from the test specimen.

2.1 Particle Connection Parameters Checking

A cylindrical body (diameter 50 mm × height 120 mm) was used to pack 3650 small particles with the same dimensions. The physical parameters of the particles and the contact parameters are shown in Table 1. The five parameters of the connection bond are listed in Table 1. In the cylinder body, 3D-models of the test specimen were compressed into 102 mm, 101 mm, 100.5 mm, 100.2 mm and 100 mm (Figure 2).

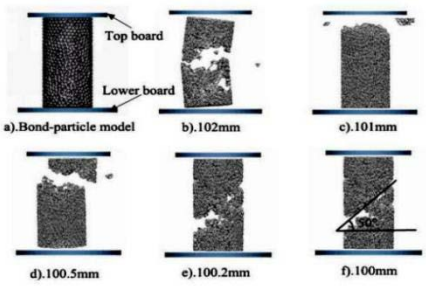

Figure 2 Test specimen crushing forms.

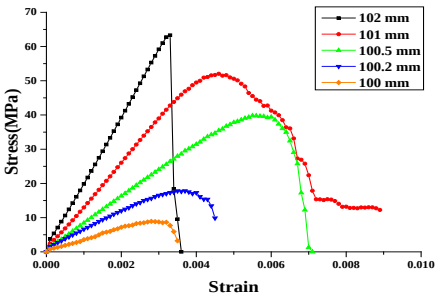

Figure 3 Stress-strain curve of specimen.

A fixed lower board and a top board with a velocity of 1 mm/s were applied in the simulation. The stress-strain curves of the five test specimens are shown in Figure 3. When the uniaxial compression test compressed to 100.2 mm, obvious elastic-plastic, strain-softening and friction stages could be seen in the stress-strain curve. The fracture surface of the specimens (Figure 2f) with an angle of about 50 degrees in the horizontal direction fits basic failure types in accordance with specimens in uniaxial compression. Finally, through theoretical formulas, the compressive strength of the specimens was calculated as 52.0 MPa, with 13.1 GPa elastic modulus.

Table 1 Summary of simulation conditions.

Material property	**Particle**	**Cylinder body**	**Collision properties**	**Particle**	**Particle-Cylinder**
Poisson ratio	0.3	0.3	Coefficient of restitution	0.2	0.25
Shear modulus	0.56 GPa	70GPa	Coefficient of static friction	0.5	0.7
Density	2630 kg/m^3	7800kg/m^3	Coefficient of rolling friction	0.001	0.001
Particle connection parameters			**value**		
Unit area normal stiffness k_b^n			9.39×10^{11} N/m^3		
Unit area shear stiffness k_b^t			4.7×10^{11}N/m^3		
Critical normal stress σ_{cr}			245 MPa		
Critical tangential stress τ_{cr}			98 MPa		
Radius of connection bond R_b			2.1 mm		

2.2 Simulation of Particle Compression Crushing

The intercepted particles from three different locations were subjected to an uniaxial compression test, as shown in Figure 4. The fragmentation of the three locations is presented in Figure 5.

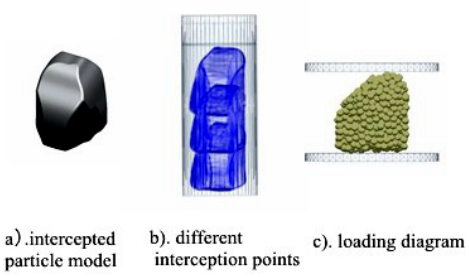

Figure 4 Intercepted particle model.

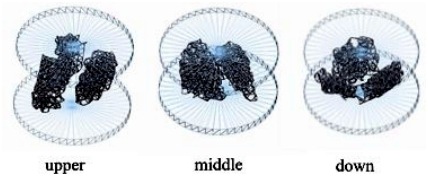

Figure 5 Fragmentation of the three locations.

The intercepted particles in different locations were broken into two or three broken grains and some powder particles. The crushing force varied with time (Figure 6). The crushing force peaked at three positions, reaching 4306.54 N, 3847.75 N and 3939.03 N, respectively.

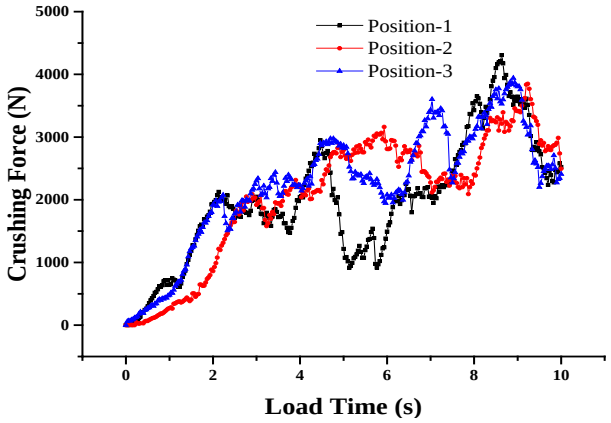

Figure 6 Crushing force variation with time.

2.3 Tests of Particle Compression Crushing

Using an electronic universal testing machine (DNS series, see Figure 7(a)), a particle crushing test was conducted, with the maximum range of the test machine load sensor at 300 kN. A computer system controlled the test machine through the Test-Expert static test software. The grain size of the granules in the test sample ranged from 30 mm to 40 mm (Figure 7(b)). The pressure head was loaded vertically downward at 5 mm/min and the loading time was 10 s (Figure 7(c)). Forty groups of particles were selected for a one-way compression test.

(a) Testing machine (b) Granite specimen (c) Uniaxial compression

Figure 7 Experimental scheme.

It was found that the maximum crushing force in the single particle compression test of each group was between about 3000 N and 4000 N (Figure 8). Secondly, under the process of unidirectional compression load there were a number of different crushing force peak points. After each peak point, with the load pressure increasing, the maximum plummeted and particle breakage occurred. Four typical crushing force-loading time curves are summarized in Figure 8. The third and fourth curve types and their corresponding crushing forms more typically reflect the crushing effect of actual rock. Comparing Figure 6 with Figure 8, regardless of the maximum crushing force, the crushing force with loading time trends and broken form were close to the actual test results, which further proves that the results obtained by the uniaxial compression particle connection model conform to the mechanical properties of actual rock material.

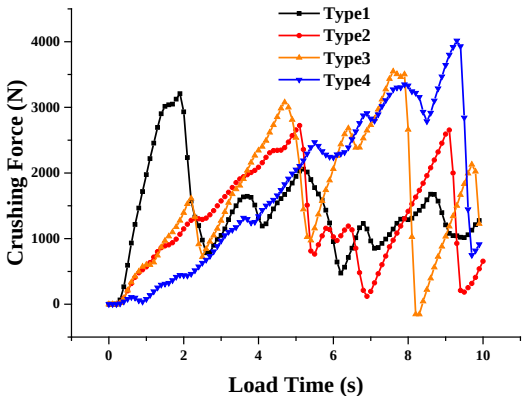

Figure 8 Crushing force variation over time in the experiment.

3 Theoretical Model and Evaluation Index of Composite Load

The theoretical model of the composite load is shown in Figure 9. Its structure mainly consists of a moving upper plate and a fixed lower plate. The related parameters of geometry and motion state directly influence the crushing. With the speed of moving plate v, the curvature of moving plate ρ_m, the curvature of fixed plate ρ_f, the space between the two plates l, and the initial radius of particle R_b as breakage parameters, the particle breaking law was investigated. At the same time, the intercepted spherical particle was selected as the research object from the single axial compression specimen.

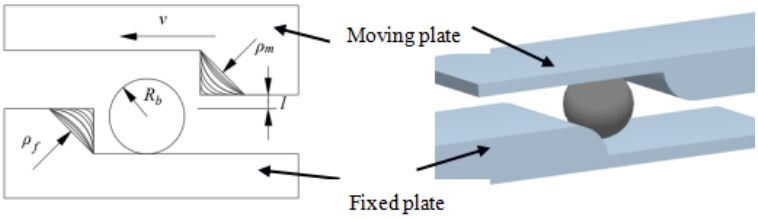

Figure 9 Crushing force variation over time in the experiment.

3.1 Evaluation of Crushing Index

Guyon, *et al.* proposed a scientific and representative classification method in their studies on particle crushing form [24,25]. There are three types of particle breakage: fracture, attrition, and abrasion (Figure 10). Fracture means that the crushed particles are approximately equally sized. Attrition means that large and small particles are created, while abrasion means that the particles are crushed into a fine powder.

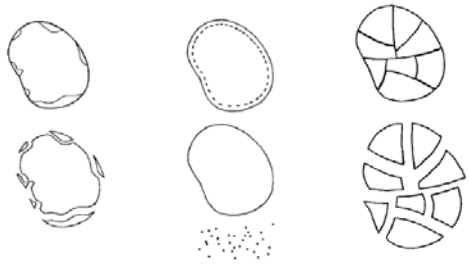

(a) Fracture (b) Attrition (c) Abrasion

Figure 10 Three types of particle breakage

The energy consumption of particle breakage is mainly work that goes from the moving plate to the particle. The moving plate is uniform in motion, $v = C$. The work can be further converted into the product of the time integral and the moving speed, as shown in Eq. (1).

$$W = v \int F(t)dt \tag{1}$$

The size and uniformity of the crushed particle directly affects the crushing performance. The crushed product usually has an irregular geometric shape. In this paper, the average size of the crushed particle ($\bar{d}$) is represented by the mean of a three-dimensional geometric value (length – l, breadth – b, height – h). The ratio between the average particle size and the original particle size (D) is defined as the breakage degree (i_s). The smaller this value, the greater the

degree of crushing. The formula is shown in Eq. (2). Breakage homogeneity (σ) can be evaluated by the mean variance of the crushed product size, as shown in Eq. (3).

$$i_s = \frac{\bar{d}}{D} = \frac{l+b+h}{3D} \tag{2}$$

$$\sigma = \sqrt{\frac{1}{N}\sum_{i=1}^{N}\left(d_i - \bar{d}\right)^2} \tag{3}$$

where σ is the breakage homogeneity, N is the number of crushed product, d_i is the size of the i-th crushed product; $\bar{d}$ is the average size of the crushed particles, and D is the original particle size.

3.2 Numerical Simulations

In order to obtain a reasonable breakage degree and breakage homogeneity, a number of simulations were carried out to improve breakage performance. Seven simulation tests were conducted in each group, with a total of 287 groups. The settings of the simulations are shown in Table 2. Through observation of the particle breakage force curve and elimination of the two largest differences, the remainder of each group was used for statistical analysis.

Table 2 Test table of single-factor particle crushing.

No.	V(m/s)	ρ_m(m)	ρ_f(m)	l(mm)	R(mm)
1-9	0.5,5,10,15,20, 25,30,35,40	25	25	23	7
10-18	20	0,6,12.5,18,25,37 .5,50,75,100	25	23	7
19-27	20	25	0,6,12.5,18,25, 37.5,50,75,100	23	7
28-36	20	25	25	21,21.5,22,22.5,2 3,23.5,24,24.5,25	7
37-45	20	25	25	23	5,5.5,6,6.5,7, 7.5,8,8.5,9

4 Discussion of Crushing Simulation with Composite Load

4.1 Influence of Moving Plate Speed

As can be seen from Figures 11(a-i), with the increase of the moving plate speed, the number of crushed particles gradually increases. The particle crushing form changes from fracture to attrition and abrasion. As can be seen

from the corresponding curves of energy consumption (Figure 12(a)), the energy consumption increased with the increasing velocity of the moving plate at speeds between 5 m/s and 20 m/s, and the particle abrasion stage and attrition stage occurred. When the moving plate speed was larger than 20 m/s, the energy consumption decreased rapidly and there was a change from the attrition stage to the fracture stage. When the moving plate speed was 30 m/s, the minimum energy consumption was achieved.

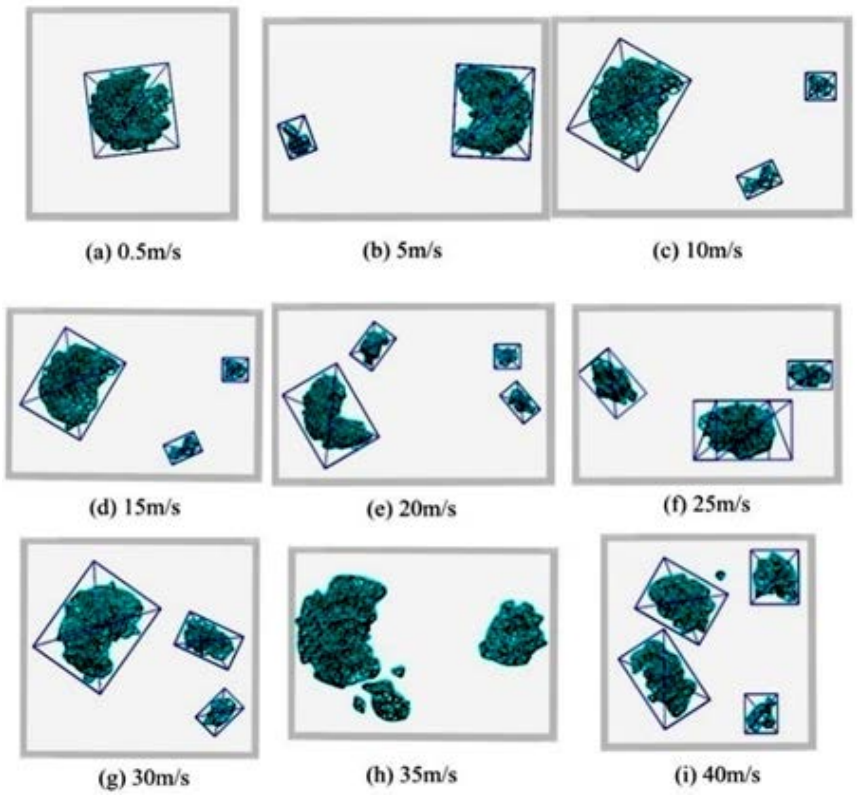

Figure 11 Particle crushing under different moving speed conditions.

The curved lines in Figures 12 and 13 represent the ever increasing speed that makes the number of crushed particles grow, which requires more energy. There is a linear relationship between the speed of the moving plate and the breakage degree. Secondly, the variance of broken product is roughly the opposite of the breakage degree. With the increase of the moving plate speed, the number of particles breaking up gradually increases and breakage uniformity decreases. A moving speed of 20 m/s, taken from the intersection in Figure 13, is the compromise value for reasonable breakage performance.

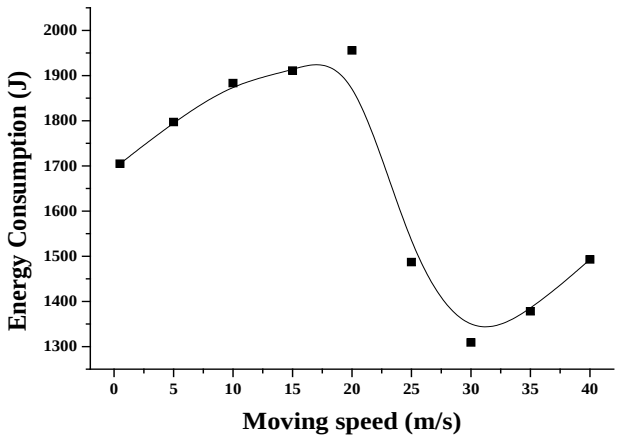

Figure 12 Curve of energy consumption against moving speed.

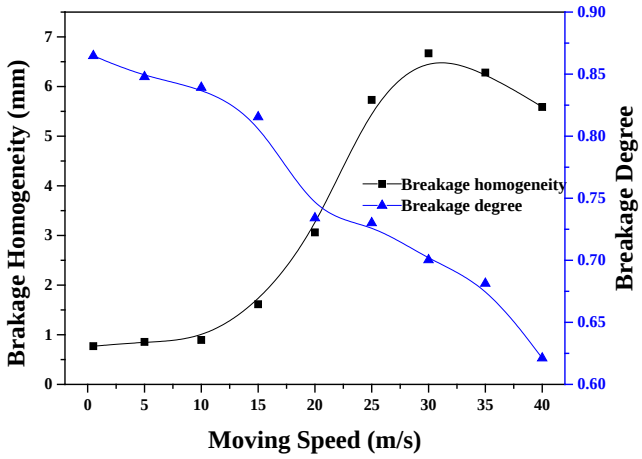

Figure 13 Curves of curshing results against moving speed

4.2 Influence of Curvature of Moving Plate ρ_m

Figure 14(a-i) shows particle crushing under different curvatures of the moving plate at a moving plate speed of 20 m/s. The crushing form is mainly fracturing. The number of crushed particles becomes higher with increasing curvature of the moving plate. When the curvature of the moving plate is 0 mm, 6 mm, or 12.5 mm, the geometrical characteristics of the moving plate are close to a 90° angle (Figure 15). The particles are chopped by the moving plate. When the curvature of the moving plate becomes larger, the geometrical characteristics are almost flat (Figure 16).

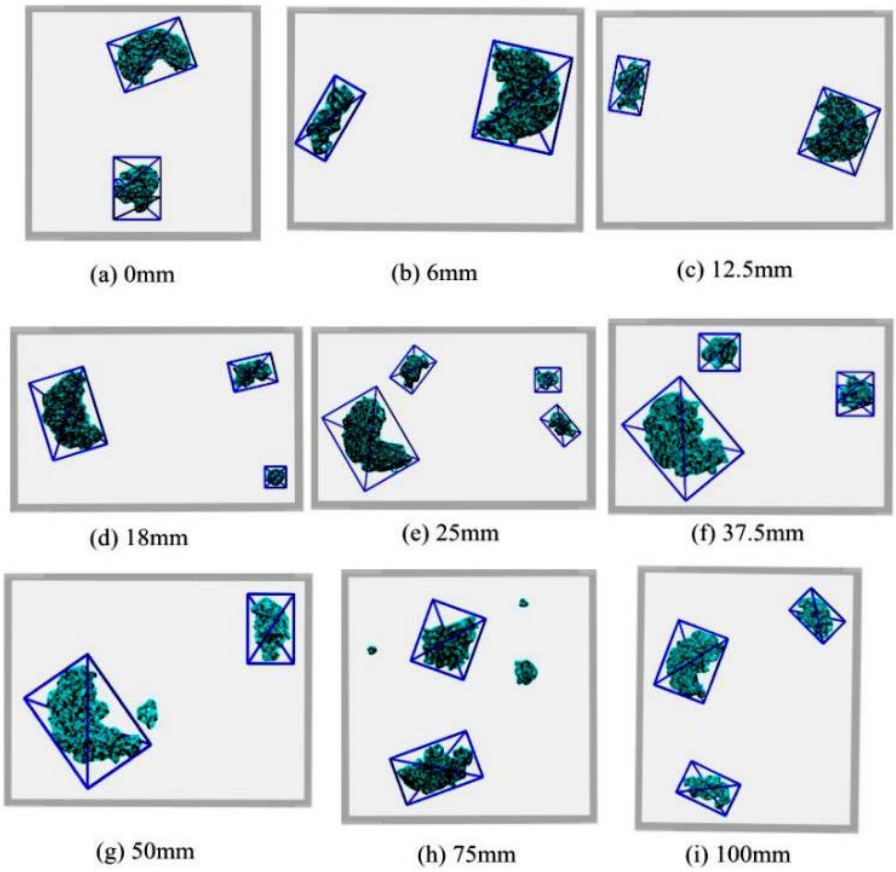

Figure 14 Particle crushing under different curvatures of the moving plate.

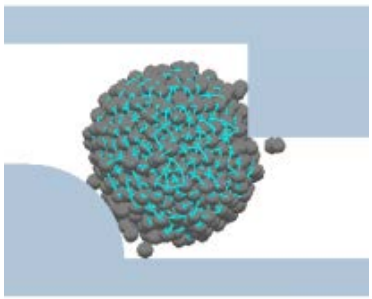

Figure 15 Curvature at 0 mm.

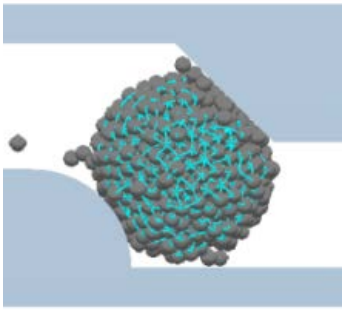

Figure 16 Curvature at 100 mm.

The particles are compressed. The energy consumption of the chopped particles is higher than that of the compressed particles, as can be seen from Figure 17. When the curvature of the moving plate is 0~12.5 mm, the crushing form is

mainly split, the crushing depth value rises, and the breakage degree decreases. The variance value of the crushing product is decreased, and the breakage homogeneity is improved (Figure 18). When the curvature of the moving plate is greater than 12.5 mm, the two trends change slowly. A curvature of the moving plate of about 25 mm, taken from the intersection in Figure 18, is the compromise value to achieve reasonable breakage performance.

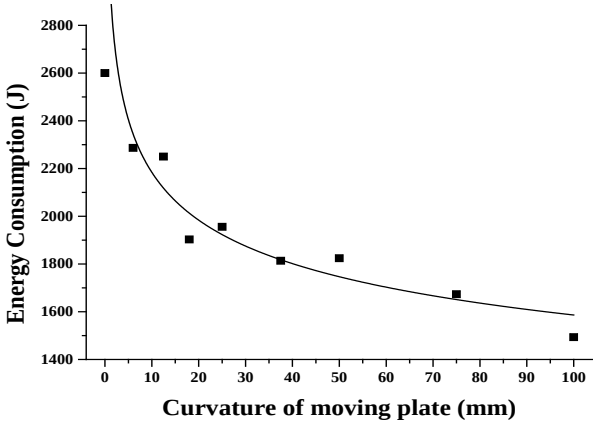

Figure 17 Curve of energy consumption against curvature of the moving plate.

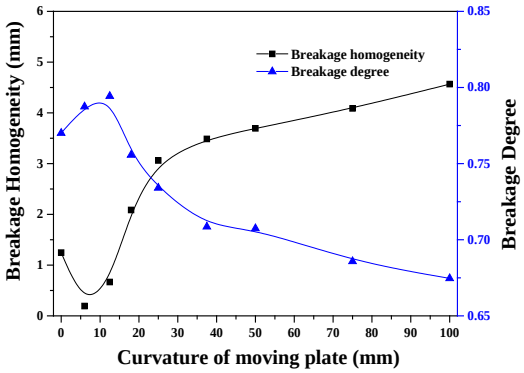

Figure 18 Curves of crushing results and curvature of the moving plate.

4.3 Influence of Curvature of Fixed Plate ρ_f

Figure 19 shows that with the curvature of the fixed plate increasing, the geometric shape changes from rectangular to a plane. An angle of 90° has a fixed effect on the particles, while abrasion is the main crushing form. When the fixed slab geometry gradually transitions to the plane, the moving plate and the fixed plate have enough time to squeeze the particles. However, because of the

increased time, the energy consumption of crushing increases. Figures 20 and 21 represent a plate curvature smaller than 18 mm. The value of the crushing depth decreases with the increase of the fixed plate curvature while the breakage degree becomes larger.

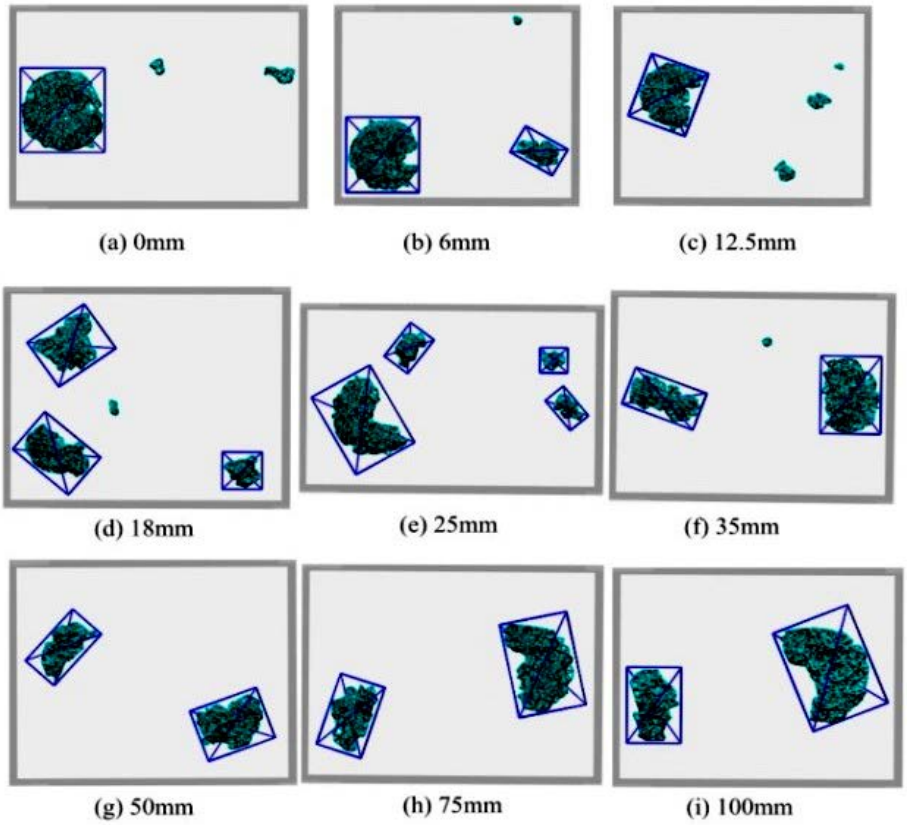

Figure 19 (a-i) Particle crushing under different curvatures of fixed plate ρ_f.

The variance of the broken product increases, the breakage homogeneity decreases, and the energy consumption decreases. When the plate curvature is larger than 18 mm, with the plate curvature increasing and the scope for granule extrusion reducing, the crushed particle size gets bigger and the breakage degree decreases slightly. At this point, the variance values of the broken product are gradually reduced, the uniformity of the broken product is increased, and the crushing energy consumption increases gradually. A curvature of the fixed plate of almost 10 mm, taken from the intersection in Figure 21, is the compromise value to achieve reasonable breakage performance.

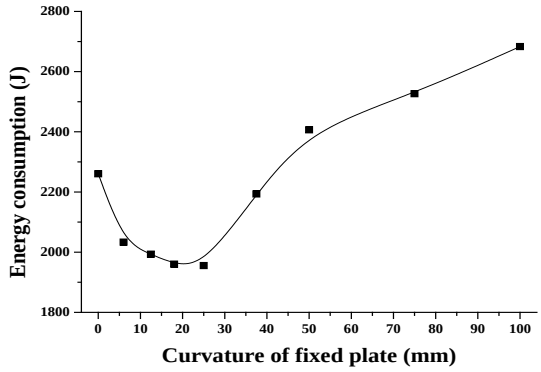

Figure 20 Curve of energy consumption against curvature of the fixed plate.

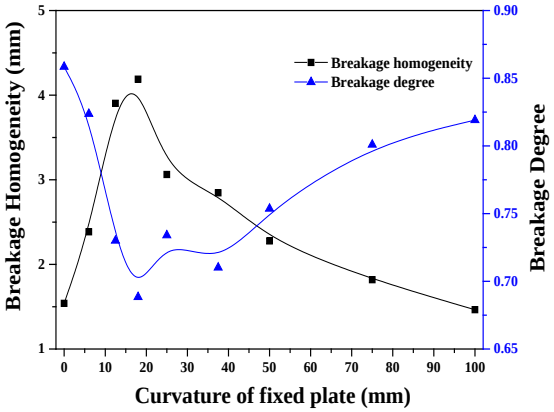

Figure 21 Curves of crushing results against curvature of the fixed plate.

4.4 Influence of Initial Particle Radius

Figure 22(a-i) represents the curve between energy consumption and the initial particle radius. Combining Figures 23 and 24, with the increase of the initial particle radius, the particles in the space between the plates get larger. The collision area becomes larger and the squeezing makes the particles fracture. Figure 23 shows the relationship between energy consumption and initial particle radius. It can be easily seen from this figure that as the initial particle radius increases, the energy consumption of particle crushing increases exponentially. This is because particles with a larger initial radius have more parallel key bonds and need a great deal of energy to overcome the bond force.

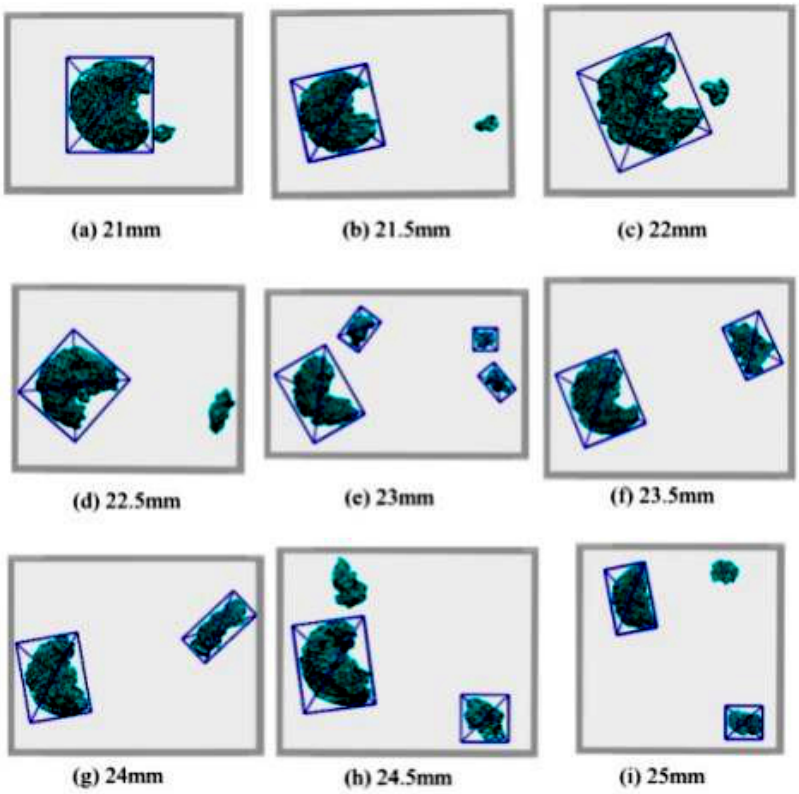

Figure 22 (a-i) Particle crushing under different initial particle radii.

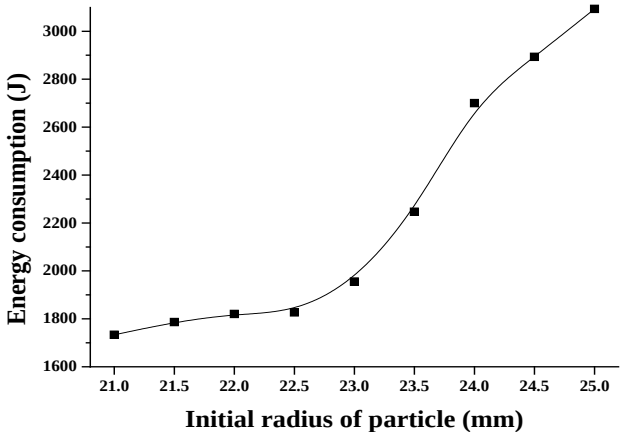

Figure 23 Curve of energy consumption against initial particle radius.

Figure 24 shows the relationship between the uniformity and breakage degree and the corresponding particle radius. With the increase of the initial radius, the particle breakage form changes from fracture to attrition. The particle energy consumption increases exponentially, while the particle breakage degree and evenness of breaking show an increasing and decreasing trend, respectively. When the initial particle radius is within the range of 22 mm to 23.5 mm, the breakage degree and the uniformity increase and decrease, respectively. An initial particle radius of almost 23 mm, taken from the intersection in Figure 24, is the compromise value to achieve reasonable breakage performance.

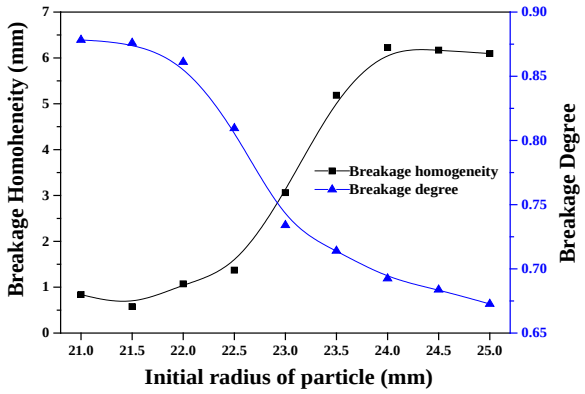

Figure 24 The curves between crushing results and initial radius of particle

4.5 Influence of Space between Plates

Figures 25(a-i) show the curve of energy consumption against the space between the two plates. Figure 26 shows a relation diagram of energy consumption and particle crushing. Compared with the other parameters, the energy consumption changes slightly under different spaces between the plates. When the space between the plates is smaller than 8 mm, the space at between 6.5 mm and 7 mm, the energy consumption reaches its minimum value. The particle crushing form changes from the fracture to the attrition. When the space is greater 8 mm, the extrusion of the moving plate increases so the energy consumption decreases, as can be seen in the graph.

Figure 27 shows the relationship between particle uniformity and crushing degree. It can be seen from the figure that, as the gap between the plates increases, the variance of the broken product and the crushing depth decrease and increase respectively. A space between the plates of almost 7.2 mm, taken from the intersection in Figure 27, is the compromise value to achieve reasonable breakage performance.

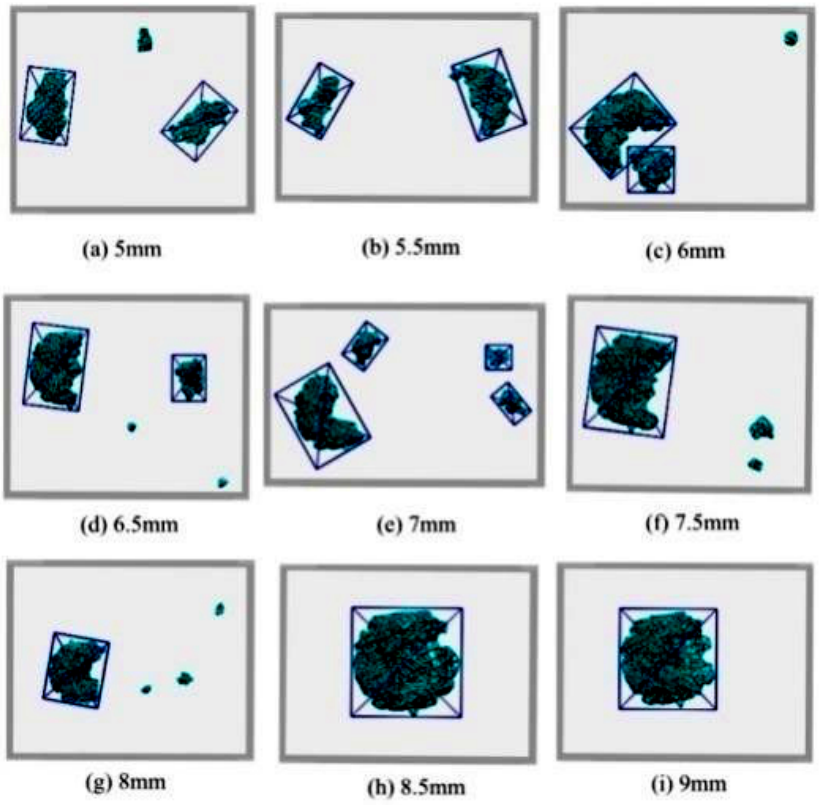

Figure 25 (a-i) Particle crushing for different space between the plates.

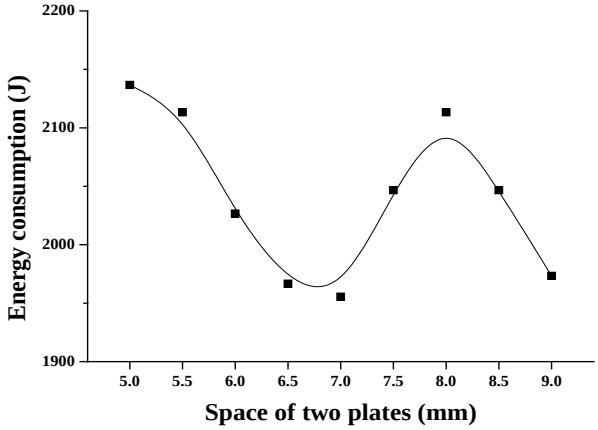

Figure 26 Curve of energy consumption against space between plates.

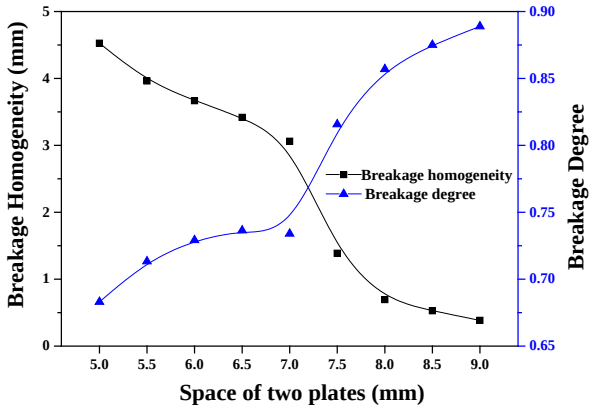

Figure 27 Curves of crushing results against space between plates

5 Conclusion

In this study, an existing particle bounding model was improved and some simulation parameters were calibrated and verified by particle crushing experiments. Meanwhile, a new coupling model containing dynamic and static loads is proposed. Particle crushing simulations were carried out with different crushing parameters. The relationships between energy consumption, degree of crushing, particle homogeneity and crushing parameters were represented by curves. The crushing mechanism was analyzed based on these curves, with the following results:

1. The changes in crushing degree and particle homogeneity are opposite to each other along the change of the variable parameters. An increase in particle crushing degree, a decrease in average particle size, and an increase in particle number all result in a decline of crushed particle homogeneity.
2. A space between plates of almost 7.2 mm, an initial particle radius of almost 23 mm, a fixed plate curvature of almost 10 mm, a moving plate curvature of about 25 mm, and a moving speed of 20 m/s are the compromise values to achieve reasonable breakage performance. When the curvature of the moving and fixed plates is greater than 37.5 mm, the rising and falling trend of all curves gradually flattens out.
3. Under these different crushing parameters, three kinds of crushing forms (fracture, attritional, abrasion) occur in the crushing process. When the crushing form changes, the curves of energy consumption, degree of crushing, and particle homogeneity reveal a fluctuation change. The study of the mechanism contributes to the design of a new type of crushing machine and provides a theoretical basis.

Acknowledgement

The authors gratefully acknowledge the support from the Industry Cooperation Project (2017H6002) of Fujian University, Fujian Natural Science Foundation (2017J01675, 2016J01722), Key Projects of Fujian Provincial Youth Natural Fund (JZ160460). No part of this paper has been published or submitted elsewhere. The authors declare that they have no conflicts of interest related to this work.

References

[1] Cleary, P.W. & Sinnott, M.D., *Simulation of Particle Flows and Breakage in Crushers Using DEM: Part 1 – Compression Crushers*, Minerals Engineering, **74**, pp. 178-197, 2015.

[2] Sinnott, M.D. & Cleary, P.W., *Simulation of Particle Flows and Breakage in Crushers Using DEM: Part 2 – Impact Crushers*, Minerals Engineering, **74**, pp. 163-177, 2015.

[3] Franklin, J.A. & Dusseault, M.B., *Rock Engineering*, New York: McGraw Hill Publishing Company, pp. 5-10, 1999.

[4] Zang, Z.C., Zhao, C.F. & Zhang, X. *Simulation Study on Influence of Load Position on Static Crushing Form of Ballasts*, Railway Engineering, **11**, pp. 152-156, 2014.

[5] Lim, W.L., McDowell, G.R. & Collop, A.C., *The Application of Weibull Statistics to the Strength of Railway Ballast*, Granular Matter, **6**(4), pp. 229-237, 2004.

[6] Hu, Z.Z. Zhuang, Y.M., Cai & T.Y., *Experimental Study on Energy Consumption and Particle Size Distribution of Single Particle Coal under Impact Crushing*, Journal of China Coal Society, **40**(S1), pp. 230-234, 2015.

[7] Weedon, D.M. & Wilson, F., *Modelling Iron Ore Degradation Using a Twin Pendulum Breakage Device*, International Journal of Mineral *Processing*, **59**, pp. 195-213, 2000.

[8] Yu, S., *The Establishment of Multi-scale Bounded Particle Model Based on Discrete Element Method and Impact Crushing Energy Consumption Analysis*, Thesis, Jiangxi University of Science and Technology, Ganzhou, China, 2015.

[9] Li, L.Y., Xu, Z.Q., Xie, H.P. & Ju, Y., *Failure Experimental Study on Energy Laws of Rock under Differential Dynamic Impact Velocities.* Journal of China Coal Society, **36**(12), pp. 2007-2011(5), 2012.

[10] Chen, T.F., Xu, J.Y., Liu, S., Wang, P. & Fang, X.Y., *Research on Rock Energy Evolution in the Process of Impact Compression Failure*, Chinese Journal of Underground Space and Engineering, S1, pp. 1477-1482, 2013.

[11] Cleary, P.W. & Morrison, R.D., *Prediction of 3D Slurry Flow within the Grinding Chamber and Discharge from a Pilot Scale SAG Mill*, Minerals Engineering, **39**, pp. 184-195, 2012.
[12] Hossain, Z., Indraratna, B., Darve, F. & Thakur, P.K., *DEM Analysis of Angular Ballast Breakage under Cyclic Loading*, Geomechanics and Geoengineering, **2**(3), pp. 175-181, 2007.
[13] Morrison, R. & Cleary, P.W., *Using DEM to Model Ore Breakage within a Pilot Scale Sag Mill,* Minerals Engineering, **17**, pp. 1117-1124, 2004.
[14] Kamali-Asl, A., Bijay, K.C., Foroutan, M., Ghazanfari, E., Cladouhos, T.T. & Stevens, M. *Stress-strain Response and Seismic Signature Analysis of Phyllite Reservoir Rocks from Blue Mountain Geothermal Field,* Geothermics, **77**, pp. 204-223, 2019.
[15] Kamali-Asl, A., Ghazanfari, E., Newell, P. & Stevens, M., *Elastic, Viscoelastic, and Strength Properties of Marcellus Shale Specimens.* Journal of Petroleum Science and Engineering, **171**, pp. 662-679, 2018.
[16] Potyondy, D.O. & Cundall, P.A., *A Bonded-particle Model for Rock*, International Journal of Rock Mechanics and Mining Sciences, **41**(8), pp. 1329-1364, 2004.
[17] Cho, N., Martin, C.D. & Sego, D.C., *A Clumped Particle Model for Rock*, International Journal of Rock Mechanics and Mining Sciences, **44**(7), pp. 997-1010, 2007.
[18] Ingrid, T. & Marte, G. *Coupled Hydro-thermo-mechanical Modeling of Hydraulic Fracturing in Quasi-brittle Rocks Using BPM-DEM*, Journal of Rock Mechanics and Geotechnical Engineering, **09**(01), pp. 92-104, 2017.
[19] Narces, J.H., Gabriel, K.P. & Luis, M.T. *Comparison of Breakage Models in DEM in Simulating Impact on Particle Beds*, **29**(3), pp. 692-706, 2018.
[20] Zhao, G.Y., Dai, B. & Ma, C., *Study of Effects of Microparameters on Macroproperties for Parallel Bonded Model*, Chinese Journal Of Rock Mechanics And Engineering, **07**, pp. 1491-1498, 2012.
[21] Zhang, L., *The Research on the Ore Crushing with High Pressure Grinding Rolls Based on Discrete Element Method*, Thesis, Xiangtan University, China, 2016.
[22] Daniel, L. & Ron, Z. *Assessing the Energy Efficiency of a Jaw Crusher,* Energy, **74**, pp. 119-130, 2014.
[23] Johannes, Q. & Carl, M.E., *Cone Crusher Modelling and Simulation Using DEM.* Minerals Engineering, **85**, pp. 92-105, 2016.
[24] Nicholas, J.B., Chen, J.F. & Jin, Y., *A Bond Model for DEM Simulation of Cementitious Materials and Deformable Structures*, Granular Matter, **16**(3), pp. 299-311, 2014.
[25] Guyon, E. & Troadec, J.P., *Du Sac de Billes Au Tas de Sable*, Odile JACOB Sciences, Paris, 1994.